Preclinical immunogenicity and protective efficacy of a SARS-CoV-2 RBD based vaccine produced with the thermophilic filamentous fungal expression system Thermothelomyces heterothallica, C1.

Albert Osterhaus (albert.osterhaus@tiho-hannover.de)
University of Veterinary Medicine Hannover, Foundation

Mariana Gonzalez-Hernandez (mariana.gonzalez.hernandez@tiho-hannover.de)
University of Veterinary Medicine Hannover, Foundation https://orcid.org/0000-0001-7019-2165

Franziska Kaiser (franziska.kaiser@tiho-hannover.de)
University of Veterinary Medicine Hannover, Foundation

Imke Steffen (Imke.Steffen@tiho-hannover.de)
University of Veterinary Medicine Hannover, Foundation

Malgorzata Ciurkiewicz (Malgorzata.Ciurkiewicz@tiho-hannover.de)
University of Veterinary Medicine Hannover, Foundation

Geert van Amerongen (amerongen@viroclinics.com)
Erasmus MC

Ronen Tchelet (rtchelet@dyadic.com)
Dyadic Netherland B.V

Mark Emalfarb (memalfarb@dyadic.com)
Dyadic International, Inc. https://orcid.org/0000-0003-4095-5445

Markku Saloheimo (markku.saloheimo@vtt.fi)
VTT Technical Research Centre of Finland Ltd

Marilyn Wiebe (marilyn.wiebe@vtt.fi)
VTT Technical Research Centre of Finland Ltd

Marika Vitikainen (marika.vitikainen@vtt.fi)
VTT Technical Research Centre of Finland Ltd

Irina Albulescu (irina.c.albulescu@gmail.com)
Faculty of Veterinary Medicine, Utrecht University

Berend-Jan Bosch (b.j.bosch@uu.nl)
Utrecht University https://orcid.org/0000-0002-3864-232X

Wolfgang Baumgärtner (Wolfgang.Baumgaertner@tiho-hannover.de)
University of Veterinary Medicine Hanover

Bart Haagmans (b.haagmans@erasmusmc.nl)
Erasmus University Medical Center https://orcid.org/0000-0001-6221-2015

Article

Keywords:

DOI: https://doi.org/

Additional Declarations: There is a conflict of interest RT and ME work for Dyadic International, Inc. and may use the vaccine for commercial use. BJB and BLH filed a patent application on coronavirus nanoparticle vaccines. Other authors have no competing interests to declare

Preclinical immunogenicity and protective efficacy of a SARS-CoV-2 RBD based vaccine produced with the thermophilic filamentous fungal expression system *Thermothelomyces heterothallica,* C1.

Mariana Gonzalez-Hernandez[1†]; Franziska Karola Kaiser[1†], Imke Steffen[1,2], Malgorzata Ciurkiewicz[3], Geert van Amerongen[4], Ronen Tchelet[5], Mark Emalfarb[5], Markku Saloheimo[6], Marilyn G. Wiebe[6], Marika Vitikainen[6], Irina C. Albulescu[7], Berend-Jan Bosch[7], Wolfgang Baumgärtner[3], Bart L. Haagmans[8], Albert D.M.E. Osterhaus[1]*

[1]Research Center for Emerging Infections and Zoonoses, University of Veterinary Medicine Hannover, Foundation, Hannover, Germany

[2]Department of Biochemistry, University of Veterinary Medicine Hannover, Foundation, Germany

[3]Department of Pathology, University of Veterinary Medicine Hannover, Foundation, Hannover, Germany

[4]Viroclinics Xplore, Schaijk, the Netherlands

[5]Dyadic International, Inc., Jupiter, Florida USA

[6]VTT Technical Research Centre of Finland Ltd., Espoo, Finland

[7]Virology Section, Infectious Diseases and Immunology Division, Department of Biomolecular Health Sciences, Faculty of Veterinary Medicine, Utrecht University, Utrecht, the Netherlands

[8]Department of Viroscience, Erasmus Medical Center, Rotterdam, the Netherlands

* Corresponding author. Email: albert.osterhaus@tiho-hannover.de

[†]These authors contributed equally to this work.

Abstract

The emergency use of vaccines has been the most efficient way to control the ongoing COVID-19 pandemic. However, the emergence of SARS-CoV-2 variants of concern has reduced the efficacy of currently used vaccines. The receptor-binding domain (RBD) of the SARS-CoV-2 spike protein is the main target for virus neutralizing (VN) antibodies. Here, we evaluated the immunogenicity and efficacy of a SARS-CoV-2 RBD vaccine candidate produced in the *Thermothelomyces heterothallica (formerly Myceliophthora thermophila)*, C1 protein expression system, in a Syrian golden hamster (*Mesocricetus auratus*) infection model. One dose of 10 µg RBD vaccine based on SARS-CoV-2 Wuhan strain, coupled to a nanoparticle in combination with aluminum hydroxide as adjuvant, efficiently induced VN antibodies and reduced viral load and lung damage upon SARS-CoV-2 challenge infection. The VN antibodies, neutralized SARS-CoV-2 variants of concern D614G, Alpha, Beta and Gamma. Our results support the use of the *Thermothelomyces heterothallica*, C1 protein expression system to produce recombinant vaccines against SARS-CoV-2 and other virus infections, in order to help overcome limitations associated with the use of mammalian expression systems.

Key words: SARS-CoV-2, receptor binding domain, RBD, vaccine, neutralizing antibodies, hamster, *Thermothelomyces heterothallica,* C1, filamentous fungus

Introduction

The ongoing COVID-19 pandemic, caused by severe acute respiratory syndrome coronavirus 2 (SARS-CoV-2), a novel member of the family *Coronaviridae,* has so far resulted in more than 600 million cases and more than 6 million deaths worldwide [1–4]. Vaccination against

SARS-CoV-2 with several new generation vaccines has successfully reduced the spread and clinical impact of COVID-19 [5–7]. Therefore, the World Health Organization has advocated vaccination as the best way to combat the ongoing pandemic [8]. Given that the spike (S) protein of coronaviruses is the main target for virus neutralizing (VN) antibodies, vaccine development efforts have largely focused on this viral protein [9,10]. The SARS-CoV-2 S protein mediates viral attachment and entry. The S protein consists of two subunits, the S1 domain harbouring the receptor binding domain (RBD), and S2 harbouring the fusion peptide[11]. Currently, the most frequent vaccine platforms used world-wide against SARS-CoV-2 are mRNA, recombinant adenovirus and subunit vaccines, based on the expression of the S protein. Unfortunately, limited production capacity, high cost of goods and logistic hurdles limit their effective use world-wide. Furthermore, largely due to escape mutations arising in the S protein, global circulation of SARS-CoV-2 variants in a partially immune population, continues to raise challenges in containing the ongoing pandemic [12]. Alternative production platforms that do not suffer from these limitations, may offer opportunities for the development of COVID-19 vaccines that can more effectively be used in low- and middle-income countries. The protein expression technology used for vaccine development in the present study is based on the use of the *Thermothelomyces heterothallica* fungus (C1). It offers a system that uses less sophisticated media and fermentation technology and produces higher yields at lower cost than mammalian cell based systems [13,14]. This technology may provide a new avenue towards a global vaccination strategy. Here we have used the Syrian golden hamster model to evaluate the immunogenicity and efficacy of SARS-CoV-2 RBD based vaccine candidates produced with the *Thermothelomyces heterothallica* C1 protein expression system.

Materials and Methods

77 ***Virus***

78 SARS-CoV-2 Wuhan strain (isolate BetaCoV/Munich/BavPat1/2020; European Virus
79 Archive Global #026 V-03883; kindly provided by Dr. C. Drosten) was obtained from a
80 clinical case in Germany diagnosed after returning from China and propagated on Vero E6
81 cells as previously described [15]**.** All virus handling was performed in a Class II Biosafety
82 Cabinet under BSL-3 conditions.

83

84 ***Illumina sequencing***

85 For deep- sequencing, RNA was extracted as described above and subsequently cDNA was
86 generated using ProtoscriptII reverse transcriptase enzyme (New England
87 BiotechnologieBioLabs) according to the manufacturer's protocol. A SARS-CoV-2 specific
88 multiplex PCR was performed as recently described [23]. In short, primers for 86 overlapping
89 amplicons spanning the entire genome were designed using primal scheme
90 (http://primal.zibraproject.org/). The amplicon length was set to 500 bp with 75 bp overlap
91 between the different amplicons. Amplicons were purified with 0.8x AMPure XP beads
92 (Beckman Coulter) and 100 ng of DNA was converted into paired-end Illumina sequencing
93 libraries using KAPA HyperPlus library preparation kit (Roche) with the KAPA unique dual-
94 indexed adapters (Roche), following the manufacturer's recommendations. The barcode-
95 labeled samples were pooled and analyzed on an Illumina sequencer V3 MiSeq flowcell
96 (2 × 300 cycles). Adapters from the paired-end sequencing reads were trimmed using
97 cutadapt (https://doi.org/10.14806/ej.17.1.200) via: cutadapt -B
98 AGATCGGAAGAGCGTCGTGTAGGGAAAGAGTG -b
99 AGATCGGAAGAGCACACGTCTGAACTCCAGTCAC --interleaved --minimum-length
100 50. The trimmed reads were aligned to the genome of Bavpat-1 with Bowtie2 [24] using
101 parameters: --no-discordant --dovetail --no-mixed --maxins 2000. Primer sequences were

102 trimmed off from the alignments by soft-clipping the leftmost 33 bases from each sequencing
103 reads using BamUtil [25] via: trimbam {bam_file} - -L 30 R 0 --clip. Variants calling was done
104 using VarScan2 [26] and SAMtools [27] via: samtools mpileup --excl-flags 2048 --excl-flags 256
105 --fasta-ref {REFERENCE_FAASTA} --max-depth 50000 --min-MQ 30 --min-BQ 30
106 {BAM_FILE} | varscan pileup2cns --min-coverage 10 --min-reads2 2 --min-var-freq 0.01 --
107 min-freq-for-hom 0.75 --p-value 0.05 --variants 1 > {snp_file}. Sequence logo were
108 generated with logomaker [28] using a custom python script. Plotting of mutation frequencies
109 was done using R and ggplot2 [29]. All scripts used for data processing are deposited in
110 GitHub: https://github.com/nicwulab/SARS-CoV-2_in_vitro_adaptation [30]. Raw sequencing
111 data has been submitted to the NIH Short Read Archive under accession number: BioProject
112 PRJNA694097.
113
114 ***Production of SARS-CoV-2 RBD in C1 fungus expression systems***
115 A DNA sequence coding for C1 endogenous CBH1 signal sequence, residues 333 to 527 of
116 the Spike (S1) glycoprotein from SARS-CoV-2 Spike S1, a Gly/Ser linker, a SpyTag
117 sequence of 13 amino acids, a Gly/Ser-linker and C-tag (EPEA) flanked by homologous
118 recombination sequences to the C1-cell DNA expression vector and MssI restriction enzyme
119 sites was designed and synthesized by GenScript (Piscataway, New Jersey, USA). The codon
120 usage was optimized for expression in *Thermothelomyces heterothallica* and the construct
121 was cloned as described in Espinosa et al. 2021 [16] and Lazo et al. 2022 [17]. Production strains
122 for the RBD-Spytag were generated in the C1 strain DNL155 with 14 deletions of native
123 protease genes as described before [16]. Fermentations were carried out at 38°C, pH 6.8 for 5
124 days as previously described [16].
125 RBD-Spytag-C-tag was purified by affinity chromatography on a CaptureSelect™ C-tag
126 affinity matrix (Thermo Fisher Scientific) as described in Espinosa et al. 2021 and Lazo et al.

127 2022 [16, 17]. The binding activity of C1 produced and C-tag affinity purified RBD-Spytag-
128 C-tag to human Angiotensin Converting Enzyme-2 (ACE2) was studied in Enzyme-Linked
129 Immunosorbent Assay (ELISA). A microtiter ELISA plate was coated with recombinant
130 human ACE2 receptor (SinoBiological) and a dilution series of RBD-Spytag protein was
131 applied on wells. Bound RBD was detected by Capture Select Biotin Anti-C-tag conjugate
132 (ThermoFisher) and the secondary detection agent was Streptavidin-HRP (Cytiva). 3,3′,5,5′-
133 tetramethylbenzidine (TMB) substrate was added and hydrolyzed in a colorimetric reaction.
134 The amount of hydrolyzed substrate is proportional to the concentration of the RBD-Spytag
135 protein present in wells. Hydrolysis reaction was stopped with sulfuric acid, A450nm was
136 measured, and results were analysed by 4-parameter logistic (4PL) analysis. C1 produced
137 RBD-C-tag without a Spytag was used as a comparison.
138
139 ***Coupling of C1 produced RBD to nanoparticles***
140 The nanoparticles mutant i301 aldolase (mi3) was used for coupling to C1 produced RBD [18].
141 SpyCatcher-mi3-Ctag recombinant protein and mi3-SpyTag-StrepTag were expressed in
142 Rosetta E. coli bacteria from ET28a (https://www.addgene.org/112255/) and pGEX-2T (GE
143 Healthcare Life Sciences). When bacterial cultures reached an OD_{600} of ~0.8 the expression
144 was induced with 0.5 mM IPTG and incubation continued overnight, at room temperature,
145 with shaking. Approx. 16 h later the bacteria were pelleted by centrifugation for 45 min/5°
146 C/4000 xg in 50 mL tubes. Each pellet was resuspended in 10 mL Lysis buffer (50 mM
147 HEPES, 150 mM NaCl, 0.1 % Tx-100, 0.1 mg/mL Lysozyme, cOmplete™ protease
148 inhibitors) and incubated for 30-60 minutes on ice. Afterwards each tube was subjected to 4
149 rounds of 30 seconds sonication to disrupt the bacteria. Unlysed bacteria and debris were
150 removed by ultracentrifugation for 45 min/5 °C/25k RPM using a SW32Ti rotor. Proteins
151 were purified from the supernatants using corresponding affinity resin: CaptureSelect™ C-

152 tag Affinity Matrix (ThermoFisher Scientific) for SpyCatcher-mi3, and Strep-Tactin®
153 Sepharose® resin (IBA-Lifesciences) for mi3-SpyTag, according to manufacturer's
154 recommendations. Concentrations of purified proteins were determined with the NanoDrop
155 ND-1000 spectrophotometer.
156 For optimizing the coupling of nanoparticles (SpyCatcher-mi2) with the RBD-SpyTag,
157 several molar ratios were tested by incubating overnight in DPBS, without calcium and
158 magnesium (Lonza), at room temperature. The molar ratio of 1:3 RBD:NP offered the best
159 coupling efficiency.
160
161 ***SDS-PAGE and Coomassie staining of antigens***
162 From each mix, 25 µL (equivalent of 2.5 µg RBD in lane 1) was mixed with 4x Laemmli
163 sample buffer, heat denatured for 10 minutes and separated on a continuous polyacrylamide
164 gel (prepared in house from 4 %, 10 % and 16 % acrylamide solutions) in running buffer
165 containing 25 mM Tris base, 190 mM glycine and 0.1 % SDS. Afterwards the gel was fixed
166 with a solution of 50 % methanol, 10 % acetic acid in water for 30 minutes. The fixative was
167 removed and the Coomassie Brilliant Blue G-250 staining solution (BioRad) was added for
168 an hour, following distaining in water overnight. The gel was scanned with the LI-COR
169 Odyssey Imaging System.
170
171 ***Animal experiment***
172 Approval for the experiment was given by the Dutch Centrale Commissie Dierproeven
173 (CCD) (Project license number 27700202114492-WP12). Ten weeks old Syrian golden
174 hamsters (*Mesocricetus auratus*) were divided into eight groups with 5 animals each, to
175 evaluate the pre-clinical efficacy of the RBD based vaccine. At day 0, serum samples were
176 collected, and the hamsters were injected intramuscularly with PBS (control group), 10 µg of

177 SARS-CoV-2 RBD, 10 µg of SARS-CoV-2 RBD coupled to a nanoparticle (RBD-nano), 10
178 µg SARS-CoV-2 RBD with the non-coupled nanoparticle. As adjuvant aluminum hydroxide
179 (alum) 2% (Croda GmbH) was used in a 2:1 antigen:alum ratio. We also evaluated the
180 antibody response of 10 µg SARS-CoV-2 RBD, RBD-nano and the RBD plus the
181 nanoparticle in combination with alum as adjuvant. Hamsters received a boost with the
182 respective vaccine candidates 28 days after the first dose. Hamsters were challenged
183 intranasally with 10^4 $TCID_{50}$ of SARS-CoV-2 42 days after the first dose of vaccination. Four
184 days post infection, the animals were humanely euthanised, necropsy was conducted, and
185 tissues were collected for further processing.
186
187 ***RT-qPCR***
188 Viral RNA was extracted using QIAmp Viral extraction kit according to the manufacturer's
189 instructions. RT-qPCR assay was performed using the protocol established by the Institut
190 Pasteur [19]. In brief, primers and probe targeting SARS-CoV-2 RdRp gene were used
191 following the Super Script III Platinum One-Step RT-qPCR (Invitrogen) protocol.
192 Amplification was performed as followed: reverse transcription 55 °C 20 min, denaturation
193 95 °C 3 min, followed by 50x cycles of amplification at 95 °C 15 s, 58 °C 30 s where data
194 was acquired. Further analysis and Cq values were determined using the Bio-Rad CFX
195 Maestro software (BioRad).
196
197 ***Virus infectivity titration***
198 Infectious SARS-CoV-2 in lung and nasal turbinate tissues was quantified in Vero cells
199 (ATCC CCL-81) in 96 well plates, as previously described [5,20]. In short, 10-fold serial
200 dilutions of homogenized tissues were used to infect the cells, starting dilution 100- and 10-
201 fold for lung and nasal turbinate homogenate, respectively. Plates were incubated in a

202 humidified atmosphere, at 37°C, 5% CO2. Cytopathic effect was evaluated 5 days post
203 infection. Virus titers ($TCID_{50}$/ml) were calculated using the Spearman-Karber method.
204
205 ***SARS-CoV-2 RBD ELISA***
206 Antibodies against SARS-CoV-2 RBD were detected via an in-house IgG ELISA, as
207 previously described [21]. In short, 96-well microtiter ELISA plates were coated with SARS-
208 CoV-2 Wuhan-Hu-1 RBD protein in PBS. Plates were incubated, blocked with 1 % skimmed
209 milk powder in PBS. After 1 h incubation at 37 °C, a 1:50 dilution of the serum samples were
210 added, plates were incubated, washed and incubated with goat anti-Syrian hamster IgG H&L
211 conjugated to horse radish peroxidase (Abcam). Next, plates were washed and TMB substrate
212 (Invitrogen) was added. Finally, after incubation 2M H_2SO_4 was added to stop the reaction
213 and optical density at 450 nm was measured using a Tecan Infinite 200 Microplate reader
214 (Tecan).
215
216 ***Virus neutralization assay***
217 VN antibodies present in the sera were detected as described previously [21,22]. In short,
218 inactivated serum samples (56 °C, 30 min) were first diluted 1:10 followed by 2-fold serial
219 dilutions. Vero cells (ATCC CCL-81) were seeded in a 96-well tissue culture plate. Diluted
220 sera were mixed with 200 $TCID_{50}$ of SARS-CoV-2 Wuhan-Hu-1 and incubated for 1 h at 37
221 °C. Serum-virus mix was added to a monolayer of Vero cells and further incubated at 37 °C,
222 5 % CO_2. After 8 h incubation, cells were fixed using 4 % PFA and incubated for 30 min at
223 room temperature. Next, PFA was removed, and cells were incubated for 15 min with 80 %
224 methanol. For staining, plates were blocked using 1 % BSA in PBS-0,05 % Tween 20 for 30
225 min at 37 °C. SARS-CoV-2 was detected using a 1:1000 dilution of rabbit polyclonal anti-
226 SARS-CoV-2 nucleocapsid (Sino Biological). After 1 h incubation at 37 °C, cells were

227 washed with PBS-0,05 % Tween 20, and incubated with a 1:1000 dilution of anti-rabbit-IgG-
228 Alexa Flour 488 (Invitrogen). Finally, cells were washed twice with PBS-0,05 % Tween 20.
229 Fluorescent cells were counted using the C.T.L. S6 Ultimate-V Analyzer and data was
230 analyzed using CTL ImmunoSpot® software. Neutralizing antibody titers are expressed as
231 the dilution that gave a 50 % reduction of stained cells (NT50).
232
233 ***Rhabdoviral pseudotype particles for virus neutralization assay***
234 Pseudotyped Vesicular stomatitis virus (VSV) particles bearing the spike protein of SARS-
235 CoV-2 variants of concern (VOC) were prepared as described previously [5]. In short,
236 replication-deficient VSV which encodes for enhanced fluorescent protein and firefly
237 luciferase (VSV*ΔG-GFP-FLuc), plasmids that encode for SARS-CoV-2-S Wuhan, D614G,
238 Alpha, Beta, Gamma, Omicron BA.1 and Omicron BA.5 variants were provided by Stefan
239 Pöhlmann. 293T cells were transfected with the desired spike protein or empty vector as
240 control. Cells were infected with VSV*ΔG-GFP-FLuc 24 h after transfection and incubated 1
241 h at 37 °C. Then, cells were washed three times with PBS, a 1:1000 dilution of supernatant
242 from I1-hybridoma cells (ATCC, CRL-2700) was added and cells were incubated for 1 h at
243 37 °C. Next, cells were washed once with PBS and fresh medium was added. Supernatant
244 was collected after an incubation period of 16-18 h, cellular debris was removed by
245 centrifugation (4500 rpm, 10 min) and aliquots of clarified supernatant were prepared and
246 stored at -80 °C until use. Pseudotyped concentration was calculated by $TCID_{50}$. VN
247 antibodies against SARS-CoV-2 variants of concern was performed as follows: Serum
248 samples were initially diluted 1:10, followed by 1:2 serial dilutions until a 1:2560 dilution.
249 Each serum sample was mixed with 200 $TCID_{50}$ of each variant and incubated for 1 h at 37
250 °C. Afterwards, serum-pseudotype particle mix was added to Vero cells. Luciferase activity
251 was measured as indication for transduction efficiency after 16-18 h incubation. For this,

252 cells were lysed using Lysis-Juice (PJK) according to the manufacturer's instructions. Next,
253 cell lysates were transferred to a white 96 well plate and firefly luciferase activity was
254 measured by using Beetle-Juice substrate (PJK) and a Tecan Infinite 200 Microplate reader.
255 Antibody titers are expressed as the dilution that gave a 50 % reduction in transduction
256 efficiency (VNT50).
257
258 ***Immunohistochemistry analysis***
259 For histopathology, left lung lobes were fixed by injection and immersion with 10% buffered
260 formalin. Tissues were subsequently embedded in paraffin and cut into 2 µm thick sections.
261 Lesions were evaluated on hematoxylin and eosin (HE) stained sections with a semiquantitative
262 scoring system described previously [31], with mild modifications. Alveolar inflammation was
263 scored as follows: 0 = no lesion; 1 = minimal, occasional small foci, less than 1 % of tissue
264 affected; 2 = mild, 2-25%; 3 = moderate, 26-50%; 4 = severe, 51-75%, 5 = subtotal, >75% of
265 tissue affected. In addition, the presence or absence of alveolar edema, hemorrhage,
266 necrosis/fibrin exudation and pneumocyte type II hyperplasia was recorded (0 = not present; 1
267 = present). Inflammatory infiltrates and necrosis in the airways (bronchi and bronchioli) were
268 scored as follows: 0 = no lesion; 1 = minimal, occasional small foci of inflammation, less than
269 1 % of tissue affected; 2 = mild, 2-25%; 3 = moderate, 26-50%; 4 = severe, 51-75%, 5 =
270 subtotal, >75% of tissue affected. In addition, the presence or absence of epithelial necrosis,
271 hyperplasia and intraluminal exudate was recorded (0 = not present; 1 = present). Assessment
272 of vascular lesions included scoring of perivascular infiltrates (0 = no; 1 = 1-2 cell layers; 2 =
273 3-5 cell layers; 3 = 6-10 cell layers; 4 = > 10 cell layers) and presence or absence of
274 vasculopathy (characterized by endothelial cell hyperplasia, endothelialitis and and mural
275 inflammatory infiltrates) and perivascular haemorrhage (0 = not present; 1 = present). The total
276 score reflects the sum of all scores for the separate compartments.

277 Immunohistochemistry for SARS-CoV-2 nucleoprotein was performed using a monoclonal
278 mouse primary antibody (Sino Biological, Peking, China-40143-MM05; dilution 1:16000,
279 incubation over night at 4°C), the Dako EnVision+ polymer system (Dako Agilent Pathology
280 Solutions) and 3,3´-Diaminobenzidine tetrahydrochloride (Sigma-Aldrich) as described
281 previously [32,33]. The amount of viral antigen was quantified separately in the alveoli and the
282 airways with a 5-tiered semiquantitative scoring system: 0 = no antigen; 1 = minimal,
283 occasional positive cells, less than 1 % of tissue affected; 2 = mild, 2-25%; 3 = moderate, 26-
284 50%; 4 = severe, 51-75%, 5 = >75% of cells immunolabelled). In addition, the presence or
285 absence of immunolabelled cells in the bronchial/bronchiolar exudate was recorded (0 = absent,
286 1 = present). The combined score is the sum of the alveolar and the airways scores. The
287 evaluation of histology and immunohistochemistry was performed by a board-certified
288 pathologist (MC), who was blinded to the group assignment. Scoring was confirmed by a
289 second board certified pathologist (WB).
290
291 ***Statistical analysis***
292 The statistical significance for the different assays was analyzed using GraphPad Prism
293 version 9 (https://www.graphpad.com).
294
295

296 **Results**

297 ***SARS-CoV-2 RBD production in the T. heterothallica, C1 protein expression system and***
298 ***coupling to nanoparticles***

299 The RBD vaccine candidate used was based on the sequence of the RBD of SARS-CoV-2
300 Wuhan-Hu-1. A synthetic gene encoding the RBD fused C-terminally with Spytag was
301 synthesized and cloned into a C1 expression vector under the *bgl8* promoter. Production
302 strains were generated based on this vector in a low-protease background C1 strain.
303 Cultivation of the production strain in a fed-batch process for 5 days resulted in production of
304 RBD-Spytag at approximately 0.45 g/l level. Single step purification of the RBD-Spytag
305 molecule with C-tag affinity chromatography yielded a preparate of moderate purity (Figure
306 1) that was used in subsequent studies. ELISA for binding to the ACE2 receptor showed clear
307 but somewhat lower binding activity as compared with a RBD preparate that was used as a
308 control. At least part of the lower binding could be explained by the lower purity of the RBD-
309 Spytag preparate. The RBD was conjugated to a nanoparticle and coupling efficiency was
310 verified using SDS-PAGE (Figure 2A).

311

312 ***SARS-CoV-2 RBD-nano based vaccines induce high levels of anti-RBD and VN antibodies***

313 Hamsters were immunized twice with RBD alone (RBD), RBD mixed with a nanoparticle
314 (RBD+ nano) or RBD coupled to a nanoparticle (RBD-nano), either with or without alum
315 (Figure 2B). Serum samples were collected on day 0, day 28 (prior receiving the booster dose
316 of the vaccine), day 42 (day of challenge) and day 46 (day of necropsy) to evaluate the
317 antibody response induced by the vaccine (Figure 2C). At day 28 after the first immunization
318 all hamsters that had received the RBD-nano with adjuvant (RBD-nano+alum) had developed
319 detectable SARS-CoV-2 RBD serum antibodies when tested by SARS-CoV-2 RBD-based
320 ELISA (Figure 3A) or virus neutralization assay (Figure 3B). These responses increased after

321 receiving the second dose (Figure 3C and D). In contrast, none of the other groups had
322 developed significant neutralizing antibody levels before virus challenge. After SARS-CoV-2
323 challenge (day 46), hamsters in the respective vaccinated groups showed variable antibody
324 responses as revealed by RBD-based ELISA and virus neutralization assay, with still
325 significantly higher levels ($p<0.0001$) in the RBD-nano with adjuvant group (Figure 3E and
326 F). Antibodies induced after receiving both vaccine doses, on day 42, neutralized D614G and
327 Alpha variants to a similar extent as the Wuhan variant, and to a lesser extent Beta and
328 Gamma variants (Figure 4A). Not unexpectedly, the antibodies induced were not able to
329 neutralize Omicron lineages BA.1 and BA.5.This was further confirmed when measuring the
330 neutralizing antibody responses from serum taken on day 46 (Figure 4B).
331
332 ***Anti-SARS-CoV-2 vaccination reduces viral titers in the lungs upon virus challenge***
333 To evaluate the efficacy of the vaccine candidates against virus infection, hamsters were
334 challenged intranasally with SARS-CoV-2 (D614G) and necropsy was conducted four days
335 post infection, where lungs and nasal turbinates were collected. To determine the presence of
336 viral RNA and infectious virus in the samples, we used RT-qPCR and virus titration
337 respectively. A 10- to 100-fold reduction in infectivity was detected in the lungs of the groups
338 that had received the RBD-nano without and with adjuvant, respectively (Figure 5B). Such
339 differences were not found in nasal turbinate samples when compared to the control group
340 (Figure 5A). However, reduction of viral titers in lung and nasal turbinates in the group who
341 received the RBD-nano+Alum was statistically significant (*$p<0.05$) when compared to viral
342 titers present in the control group. At the RNA level no apparent differences among the
343 groups were observed (data not shown).
344 Next, lungs, and nasal turbinates preserved in 10 % formalin were examined for
345 histopathological changes and viral antigen expression. We observed that hamsters

346 immunized with the adjuvanted RBD-nano+Alum showed significant reduction in viral
347 antigen detected in the lungs, associated with reduction of lesions (Figure 6), which was not
348 the case for the nasal turbinates.
349
350 **Discussion**
351 Like for other coronaviruses, the S protein of SARS-CoV-2 is highly immunogenic and the
352 main target of neutralizing antibodies. Hence, it has been used as the main antigen for most of
353 the vaccines developed. Depending on the platform used for vaccine production, full length
354 SARS-CoV-2-S-based vaccines may confer between 65-95 % protection in humans[34].
355 Vaccines based on mRNA expressing the S protein are among the best to induce VN
356 antibodies and provide protection against SARS-CoV-2 associated disease. These vaccines,
357 to varying degrees, also induce antibodies that cross neutralize newly arisen variants of
358 concern and reduce severe disease manifestations caused by these variants [35]. However, some
359 of the major disadvantages of these vaccines are the relative manufacturing complexity, high
360 production costs and stringent cold-chain requirements, which collectively limit their
361 applicability, especially in low-and-middle-income countries. New generation vaccines based
362 on purified S protein produced in a fungal expression system like the *Thermothelomyces*
363 *heterothallica,* C1 system, would not have these disadvantages.
364 Here, we evaluated the immunogenicity and efficacy of a SARS-CoV-2 RBD based vaccine
365 candidate expressed in the C1 fungal system using Syrian golden hamsters as animal model.
366 Our C1-RBD-Spytag-based vaccine candidate was produced at about 0.45 g/L concentrations
367 under so far non-optimized fungal fermentation conditions which resulted in a product that
368 would not require stringent cold chain conditions. Recently, the production level of C1-RBD
369 reached > 2 g/l in a 5-day fermentation (data not shown). Moreover, in the study done by
370 Ramot *et. al.*, it was shown that in New Zealand rabbits, the SARS-CoV-2- RBD produced

371 with the C1 system, did not induced any adverse effects or systemic toxicity and induced the
372 production IgG antibodies against SARS-CoV-2[36]. Furthermore, Lazo and colleagues, proved
373 that immunization with SARS-CoV-2-RBD produced in the C1 system, induced a similar
374 humoral response in mice as recombinant SARS-CoV-2-RBD produced in HEK293 cells [17].
375 We also showed that one single immunization with the RBD-nano with alum quite efficiently
376 induced SARS-CoV-2 neutralizing antibodies to higher levels than the non-adjuvanted
377 equivalent. Dalvie and colleagues also showed that when using alum as an adjuvant with
378 RBD based viral like particles as a vaccine, the induction of VN antibodies proved to be more
379 efficient than the CpG adjuvanted alternative [37,38]. These results are in partial disagreement
380 with those by Merkuleva and colleagues who evaluated the immune response induced by a
381 trimeric uncoupled RBD based candidate vaccine expressed in mammalian cells in different
382 animal models. They showed a dose dependent virus VN antibody response in the hamster
383 model, that however proved to be inferior to responses found in other animal models [39]. In
384 our hands coupling of the SARS-CoV-2 RBD to a nanoparticle proved to be crucial for the
385 induction of high titre VN antibodies and protection, as we have shown previously for a
386 MERS-CoV candidate vaccine in different animal species [13]. It is however puzzling to note,
387 that in spite of inducing high levels of VN antibody in the group that received the RBD-
388 nano+alum vaccine, the reduction of virus infectivity (10 to 100 fold) in the lungs was less
389 pronounced than that observed when golden Syrian hamsters are pre-treated with human
390 monoclonal antibodies against SARS-CoV-2, that resulted in similar VN antibody titers [40].
391 The reduction of virus infectivity titres in the lungs of hamsters vaccinated with candidate
392 alum adjuvanted RBD-nano vaccine did reach statistical significance when compared to the
393 alum control group. This was also observed when comparing viral antigen levels (Figure 6B)
394 and lesions in the lungs (Figure 6A). Reduction of virus infectivity titres and lesions were not
395 observed in the nasal turbinates. Similar results have been obtained by other groups using the

396 Syrian hamster model, Dalvie and colleagues showed that hamsters that received the RBD
397 vaccine recovered faster than the control group [38]. Moreover, in the study conducted by Chiba
398 *et. al.* it was shown that a SARS-CoV-2-S based vaccine coupled to a nanoparticle conferred
399 full protection against SARS-CoV-2 challenge in hamsters [38,41].
400 Due to the continuous emergence of VOCs, it is important to know to what extent a vaccine
401 provides cross-protection against arising virus mutants, and especially VOCs. Therefore, we
402 also evaluated the cross-neutralizing capacities of the hamster serum antibodies induced by
403 the RBD-nano+alum, our most efficient vaccine candidate, against different VOCs in a VSV
404 pseudotype-based virus neutralization assay. We showed that even though most of the
405 relevant VOC mutations are located within the RBD, the induced hamster serum antibodies
406 appeared to neutralize some of the VOCs tested, albeit with different efficiency. Moreover,
407 the induced antibodies did not cross neutralize the recent Omicron (lineage BA-1 and BA.5)
408 variants. This means that a vaccine based on this technology, would also need to be bivalent
409 or updated, in order to match the coupled RBD to that of the currently circulating variants.
410 Interestingly, the C1 vaccine platform, would allow to exchange the SARS-CoV-2 RBD in
411 short time and with high yields. In a recent study Walls and colleagues showed that the VN
412 antibodies induced by an RBD vaccine or the full S protein, exhibited different neutralization
413 efficacy depending on the animal model used. Neutralizing antibodies induced in mice
414 showed better cross neutralization against Beta and Gamma VOCs (only 2-fold reduction
415 efficiency) than VN antibodies induced in non-human primates (NHP) which were ~6-8-fold
416 less efficient in neutralizing these VOCs [42]. In our study, we also observed that neutralizing
417 antibodies induced in hamsters are affected by VOCs in a similar way as in NHP (~10-fold
418 reduction in neutralization). Most importantly, these reduced responses against some variants,
419 seen in NHPs and in hamsters, probably better reflect what has been observed in most human
420 vaccine studies [35,43,44]. Collectively our data show that it is important to consider the way the

421 antigen is presented, as well as the animal model in which vaccines are being tested, since the
422 immune response observed even within hamsters appears to vary considerably from one
423 study to another.
424 Taken together, we have shown that an adjuvanted C1 RBD-nano+alum based vaccine
425 induces potent VN antibodies, and results in reduced viral load and lung damage upon
426 subsequent SARS-CoV-2 infection in hamsters. Given the advantages of this approach, it
427 should be further evaluated as an alternative vaccine development strategy that may
428 overcome some of the limitations of the current COVID-19 vaccines and vaccine candidates,
429 and therefore make it more applicable for low- and middle-income countries.

430 **Acknowledgements**

431 We thank Kristin Laudeley and Margarethe Jentzsch for their technical support. This study
432 was performed as part of the Zoonotic Anticipation and Preparedness Initiative (ZAPI
433 project) [Innovative Medicines initiative (IMI) grant 115760], with assistance and financial
434 support from IMI and the European Commission and contributions from EFPIA partners.
435 B.L.H., is supported by the NIH/NIAID Centers of Excellence for Influenza Research and
436 Response (CEIRR) under contract 75N93021C00014-Icahn School of Medicine at Mt. Sinai.
437 This research was also funded by the Deutsche Forschungsgemeinschaft (DFG; German
438 Research Foundation AO, FKK, IS,WB, -398066876/GRK 2485/1; Ministry of Science and
439 Culture of Lower Saxony in Germany (14 – 76103–184 CORONA-15/20, WB and AO); and
440 by the COVID-19 Research Network of the State of Lower Saxony (COFONI) with funding
441 from the ministry of science and culture of Lower Saxony, Germany (14–76403–184, MC,
442 WB). This Open Access publication was funded by the Deutsche Forschungsgemeinschaft
443 (DFG, German Research Foundation) -491094227 “Open Access Publication Costs” and the
444 University of Veterinary Medicine

Hannover, Foundation. ICA was funded through the Utrecht Molecular Immunology Hub (Utrecht University).

Author contributions

Production, expression and coupling of RBD, RT, ME, MS, MGW, MV, ICA, BJB; animal experiments, MGH, FKK and GvA; pathological investigation, WB, MC; supervision ADMEO, BLH; VNT and VSVpp MGH, FKK, IS; study conception and coordination, ADMEO, BLH, RT; manuscript writing, MGH, FKK, ADMEO with input from all other authors.

Disclosure statement

RT and ME work for Dyadic International, Inc. and may use the vaccine for commercial use. BJB and BLH filed a patent application on coronavirus nanoparticle vaccines. Other authors have no competing interests to declare.

Data availability

All data needed to evaluate the conclusions in this paper are present in the paper.

References

1. Center for Systems Science and Engineering, J. H. U. COVID-19 Dashboard. https://coronavirus.jhu.edu/map.html (2021).
2. WHO. Coronavirus disease (COVID-19) pandemic. https://covid19.who.int/ (2022).
3. Gorbalenya, A. E. *et al.* The species Severe acute respiratory syndrome-related coronavirus: classifying 2019-nCoV and naming it SARS-CoV-2. *Nat Microbiol* **5**, 536–544 (2020).
4. Ning, S., Yu, B., Wang, Y. & Wang, F. SARS-CoV-2: Origin, Evolution, and Targeting Inhibition. *Front Cell Infect Microbiol* **11**, 1–19 (2021).
5. Du, W. *et al.* An ACE2-blocking antibody confers broad neutralization and protection against Omicron and other SARS-CoV-2 variants of concern. *Sci Immunol* eabp9312 (2022) doi:10.1126/sciimmunol.abp9312.
6. Gu, C. *et al.* A human antibody of potent efficacy against SARS-CoV-2 in rhesus macaques showed strong blocking activity to B.1.351. *MAbs* **13**, (2021).
7. Kim, C. *et al.* A therapeutic neutralizing antibody targeting receptor binding domain of SARS-CoV-2 spike protein. *Nat Commun* **12**, 1–10 (2021).
8. WHO. COVID-19 advice for the public: Getting vaccinated. *https://www.who.int/emergencies/diseases/novel-coronavirus-2019/covid-19-vaccines/advice* (2022).

480 9. Huo, J. *et al.* Neutralizing nanobodies bind SARS-CoV-2 spike RBD and block
481 interaction with ACE2. *Nat Struct Mol Biol* **27**, 846–854 (2020).
482 10. Merkuleva, I. A. *et al.* Are Hamsters a Suitable Model for Evaluating the
483 Immunogenicity of RBD-Based Anti-COVID-19 Subunit Vaccines? *Viruses* **14**,
484 (2022).
485 11. Hoffmann, M. *et al.* SARS-CoV-2 Cell Entry Depends on ACE2 and TMPRSS2 and Is
486 Blocked by a Clinically Proven Protease Inhibitor. *Cell* **181**, 271-280.e8 (2020).
487 12. Zella, D. *et al.* The variants question: what is the problem? *J Med Virol* 0–2 (2021)
488 doi:10.1002/jmv.27196.
489 13. Beer, M. *et al.* Zoonoses Anticipation and Preparedness Initiative, Stakeholders
490 Conference, February 4 & 5, 2021. in (2021).
491 14. Visser, H. *et al.* RESEARCH: Development of a mature fungal technology and
492 production platform for industrial enzymes based on a Myceliophthora thermophila
493 isolate, previously known as Chrysosporium lucknowense C1. *Industrial*
494 *Biotechnology* **7**, 214–223 (2011).
495 15. Chu, H. *et al.* Comparative tropism, replication kinetics, and cell damage profiling of
496 SARS-CoV-2 and SARS-CoV with implications for clinical manifestations,
497 transmissibility, and laboratory studies of COVID-19: an observational study. *Lancet*
498 *Microbe* **1**, e14–e23 (2020).
499 16. Espinosa, L. A. *et al.* In-solution buffer-free digestion allows full-sequence coverage
500 and complete characterization of post-translational modifications of the receptor-
501 binding domain of SARS-CoV-2 in a single ESI–MS spectrum. *Anal Bioanal Chem*
502 **413**, 7559–7585 (2021).
503 17. Lazo, L. *et al.* A recombinant SARS-CoV-2 receptor-binding domain expressed in an
504 engineered fungal strain of Thermothelomyces heterothallica induces a functional
505 immune response in mice. *Vaccine* **40**, 1162–1169 (2022).
506 18. Bruun, T. U. J., Andersson, A. M. C., Draper, S. J. & Howarth, M. Engineering a
507 Rugged Nanoscaffold to Enhance Plug-and-Display Vaccination. *ACS Nano* **12**, 8855–
508 8866 (2018).
509 19. Corman, V. M. *et al.* Detection of 2019 novel coronavirus (2019-nCoV) by real-time
510 RT-PCR. *Eurosurveillance* **25**, (2020).
511 20. Armando, F. *et al.* SARS-CoV-2 Omicron variant causes mild pathology in the upper
512 and lower respiratory tract of hamsters. *Nat Commun* **13**, 3519 (2022).
513 21. Schulz, C. *et al.* SARS-CoV-2 specific antibodies in domestic cats in Europe during
514 the first COVID-19 wave. *Emerg Infect Dis* (2021).
515 22. Jonczyk, R. *et al.* Combined Prospective Seroconversion and PCR Data of Selected
516 Cohorts Indicate a High Rate of Subclinical SARS-CoV-2 Infections-an Open
517 Observational Study in Lower Saxony, Germany. *Microbiol Spectr* **10**, e0151221
518 (2022).
519 23. Oude Munnink, B. B. *et al.* Rapid SARS-CoV-2 whole-genome sequencing and
520 analysis for informed public health decision-making in the Netherlands. *Nat Med* **26**,
521 1405–1410 (2020).
522 24. Langmead, B. & Salzberg, S. L. Fast gapped-read alignment with Bowtie 2. *Nat*
523 *Methods* **9**, 357–9 (2012).
524 25. Jun, G., Wing, M. K., Abecasis, G. R. & Kang, H. M. An efficient and scalable
525 analysis framework for variant extraction and refinement from population-scale DNA
526 sequence data. *Genome Res* **25**, 918–25 (2015).
527 26. Koboldt, D. C. *et al.* VarScan 2: somatic mutation and copy number alteration
528 discovery in cancer by exome sequencing. *Genome Res* **22**, 568–76 (2012).

529 27. Li, H. *et al.* The Sequence Alignment/Map format and SAMtools. *Bioinformatics* **25**,
530 2078–9 (2009).
531 28. Tareen, A. *et al.* MAVE-NN: learning genotype-phenotype maps from multiplex
532 assays of variant effect. *Genome Biol* **23**, 98 (2022).
533 29. Wickham, H. Programming with ggplot2. in 241–253 (2016). doi:10.1007/978-3-319-
534 24277-4_12.
535 30. Wu, Y. *et al.* A recombinant spike protein subunit vaccine confers protective immunity
536 against SARS-CoV-2 infection and transmission in hamsters. *Sci Transl Med* **13**,
537 (2021).
538 31. Bošnjak, B. *et al.* Intranasal Delivery of MVA Vector Vaccine Induces Effective
539 Pulmonary Immunity Against SARS-CoV-2 in Rodents. *Front Immunol* **12**, 772240
540 (2021).
541 32. Becker, K. *et al.* Vasculitis and Neutrophil Extracellular Traps in Lungs of Golden
542 Syrian Hamsters With SARS-CoV-2. *Front Immunol* **12**, 640842 (2021).
543 33. Allnoch, L. *et al.* Vascular Inflammation Is Associated with Loss of Aquaporin 1
544 Expression on Endothelial Cells and Increased Fluid Leakage in SARS-CoV-2
545 Infected Golden Syrian Hamsters. *Viruses* **13**, (2021).
546 34. Feikin, D. R. *et al.* Duration of effectiveness of vaccines against SARS-CoV-2
547 infection and COVID-19 disease: results of a systematic review and meta-regression.
548 *The Lancet* **399**, 924–944 (2022).
549 35. Luczkowiak, J. *et al.* Neutralizing response against SARS-CoV-2 variants 8 months
550 after BNT162b2 vaccination in naïve and COVID-19 convalescent individuals. *J Infect*
551 *Dis* (2021) doi:10.1093/infdis/jiab634.
552 36. Ramot, Y. *et al.* Toxicity and Local Tolerance of a Novel Spike Protein RBD Vaccine
553 Against SARS-CoV-2, Produced Using the C1 Thermothelomyces Heterothallica
554 Protein Expression Platform. *Toxicol Pathol* **50**, 294–307 (2022).
555 37. Routhu, N. K. *et al.* SARS-CoV-2 RBD trimer protein adjuvanted with Alum-3M-052
556 protects from SARS-CoV-2 infection and immune pathology in the lung. *Nat Commun*
557 **12**, 1–15 (2021).
558 38. Dalvie, N. C. *et al.* Engineered SARS-CoV-2 receptor binding domain improves
559 manufacturability in yeast and immunogenicity in mice. *Proc Natl Acad Sci U S A* **118**,
560 (2021).
561 39. Merkuleva, I. A. *et al.* Are Hamsters a Suitable Model for Evaluating the
562 Immunogenicity of RBD-Based Anti-COVID-19 Subunit Vaccines? *Viruses* **14**, 1060
563 (2022).
564 40. Du, W. *et al.* An ACE2-blocking antibody confers broad neutralization and protection
565 against Omicron and other SARS-CoV-2 variants of concern. *Sci Immunol* eabp9312
566 (2022) doi:10.1126/sciimmunol.abp9312.
567 41. Chiba, S. *et al.* Multivalent nanoparticle-based vaccines protect hamsters against
568 SARS-CoV-2 after a single immunization. *Commun Biol* **4**, 2–10 (2021).
569 42. Walls, A. C. *et al.* Distinct sensitivities to SARS-CoV-2 variants in vaccinated humans
570 and mice. *Cell Rep* 111299 (2022) doi:10.1016/j.celrep.2022.111299.
571 43. Garcia-Beltran, W. F. *et al.* Multiple SARS-CoV-2 variants escape neutralization by
572 vaccine-induced humoral immunity. *Cell* **184**, 2372-2383.e9 (2021).
573 44. Stamatatos, L. *et al.* mRNA vaccination boosts cross-variant neutralizing antibodies
574 elicited by SARS-CoV-2 infection. *Science* (2021) doi:10.1126/science.abg9175.
575
576

577 **Figure legends**

578 Figure 1. Production of RBD-Spytag in C1 fermentation process and C-tag-affinity-purified
579 RBD-Spytag analyzed in SDS-PAGE with Coomassie Blue dye staining**.** Lane 1: MW
580 protein marker, lane 2: 98 h fermentation supernatant, lane 3: 116 h fermentation supernatant
581 which is the starting material for the affinity purification, lanes 4-6: final purified and
582 dialyzed RBD-Spytag protein as three different amounts loaded in SDS-PAGE. The RBD-
583 Spytag, corresponding to the correct size of 24 kDa protein, is marked with an arrow.
584
585 Figure 2. Analysis of antigens used for immunization and immunization scheme. A) SDS-
586 PAGE analysis was performed on the SARS-CoV-2 spike RBD antigens or RBD/nanoparticle
587 mixtures used for immunization (left panel). For comparison, nanoparticles were also analyzed
588 separately (right panel). Asterisks indicate contaminating yeast proteins. The abbreviations ST,
589 SC and NP stand for SpyTag, SpyCatcher and nanoparticles, respectively. B) Antigen
590 combinations tested in the Syrian hamster model. C) Schematic representation of the study
591 design (Created with BioRender.com).
592
593 Figure 3. SARS-CoV-2 RBD-nano vaccine induces high neutralizing antibodies titers.
594 Antibodies induced by the different vaccine formulations and neutralizing antibodies titers
595 were quantified at A-B) 28 days, C-D) 42 days after receiving the first immunization dose and
596 E-F) at the day of necropsy 46 days after immunization. IgG antibodies (A, C, E) were detected
597 by RBD-ELISA, dotted lines indicate the assay cut-off value ($\bar{x} + 2SD$) based on the control
598 group. Neutralizing antibodies titers (B, D, F) are expressed as the reciprocal of the dilution
599 that gave a 50% reduction of stained cells. P values were calculated by a two-way ANOVA
600 test, mean ± SD are presented. ****p<0.0001; ***p<0.001; **p<0.01; *p<0.05; ns not
601 significant.
602

603 Figure 4. Neutralizing antibodies induced by SARS-CoV-2 RBD-nano vaccine neutralize some
604 SARS-CoV-2 VOCs. Virus neutralization assay against D614G, Alpha, Beta, Gamma, and
605 Omicron and Omicron BA.5 variants of concern was done using vesicular stomatitis virus
606 pseudotyped with the respective spike protein. Titers are expressed as the reciprocal dilution
607 that reduced entry to 50%. P values were calculated using a one-way ANOVA analysis.
608 ****$p<0.0001$; ***$p<0.001$; **$p<0.01$; *$p<0.05$; ns not significant.
609
610 Figure 5. Viral load in the lung is reduced after vaccination with RBD-nano plus adjuvant.
611 Viral titers were calculated in A) nasal turbinate and B) lung using $TCID_{50}$. P values were
612 calculated using a Brown-Forsythe and Welch ANOVA test. ****$p<0.0001$; ***$p<0.001$;
613 **$p<0.01$; *$p<0.05$; ns not significant.
614
615 Figure 6. Histopathological lesions and viral antigen in the lungs of SARS-CoV-2 infected
616 hamsters. A and B) Representative images of a PBS-treated infected control hamster showing
617 multifocal areas of inflammation in alveoli (black arrowheads and inset in A) associated with
618 abundant viral antigen in pneumocytes (brown signal, black arrowheads and inset in B).
619 Inflammatory infiltrates are also present in the airways (white arrowheads in A), but only
620 occasional bronchial epithelial cells are positive for viral antigen (white arrowheads in B). C)
621 and D) Representative image of a hamster vaccinated with an RBD vaccine (RBD-nano+Alum)
622 showing inflammatory lesions and viral antigen exclusively in the main airways (white
623 arrowheads, inserts). A) and C): hematoxylin and eosin stain. B) and D) immunohistochemistry
624 for SARS-CoV-2 nucleocapsid protein. Insets show 400x magnification of areas delineated by
625 rectangles in the overview images. E) Semiquantitative score of histological lesions induced
626 by SARS-CoV-2 infection. F) Semiquantitative score of SARS-CoV-2 antigen present in

627 alveoli and airways. P values for were calculated using a one-way ANOVA analysis.

628 ****$p<0.0001$; ***$p<0.001$; **$p<0.01$; *$p<0.05$; ns not significant.

629
630

Figures

Figure 5.

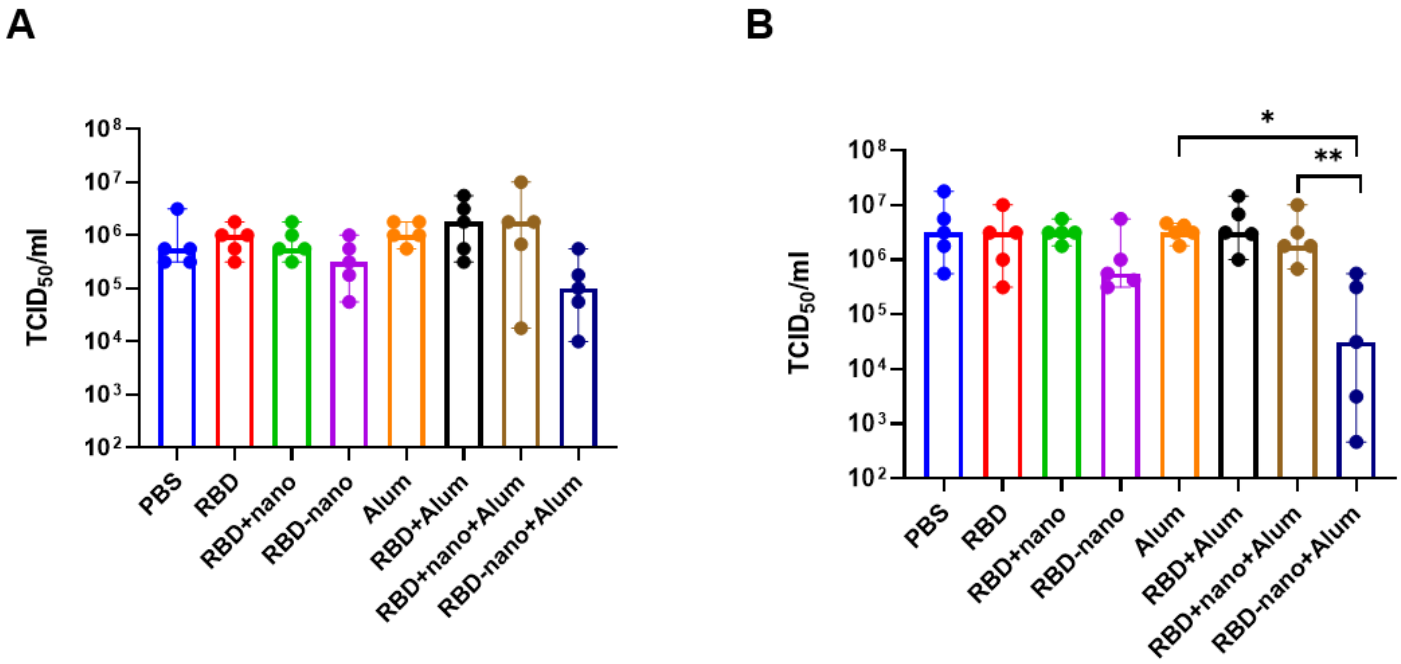

Figure 1

Figure 5

Figure 4

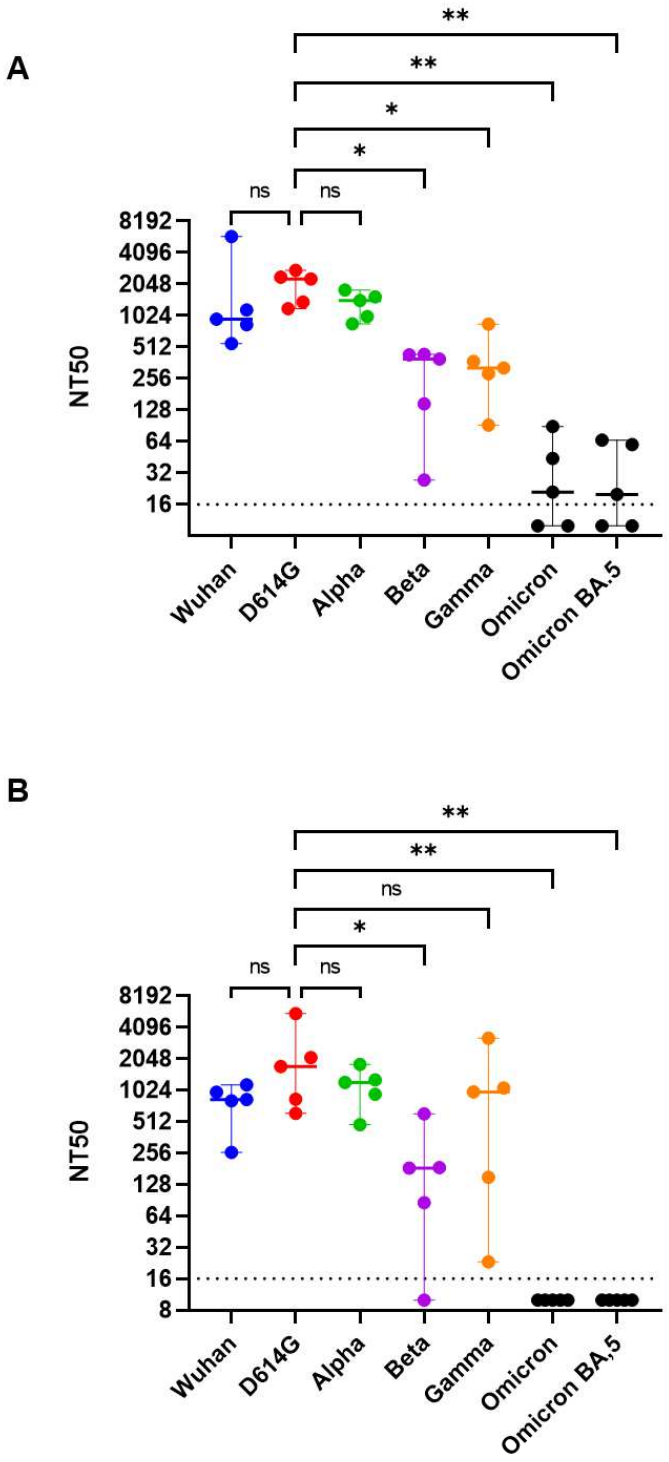

Figure 2

Figure 4

Figure 3

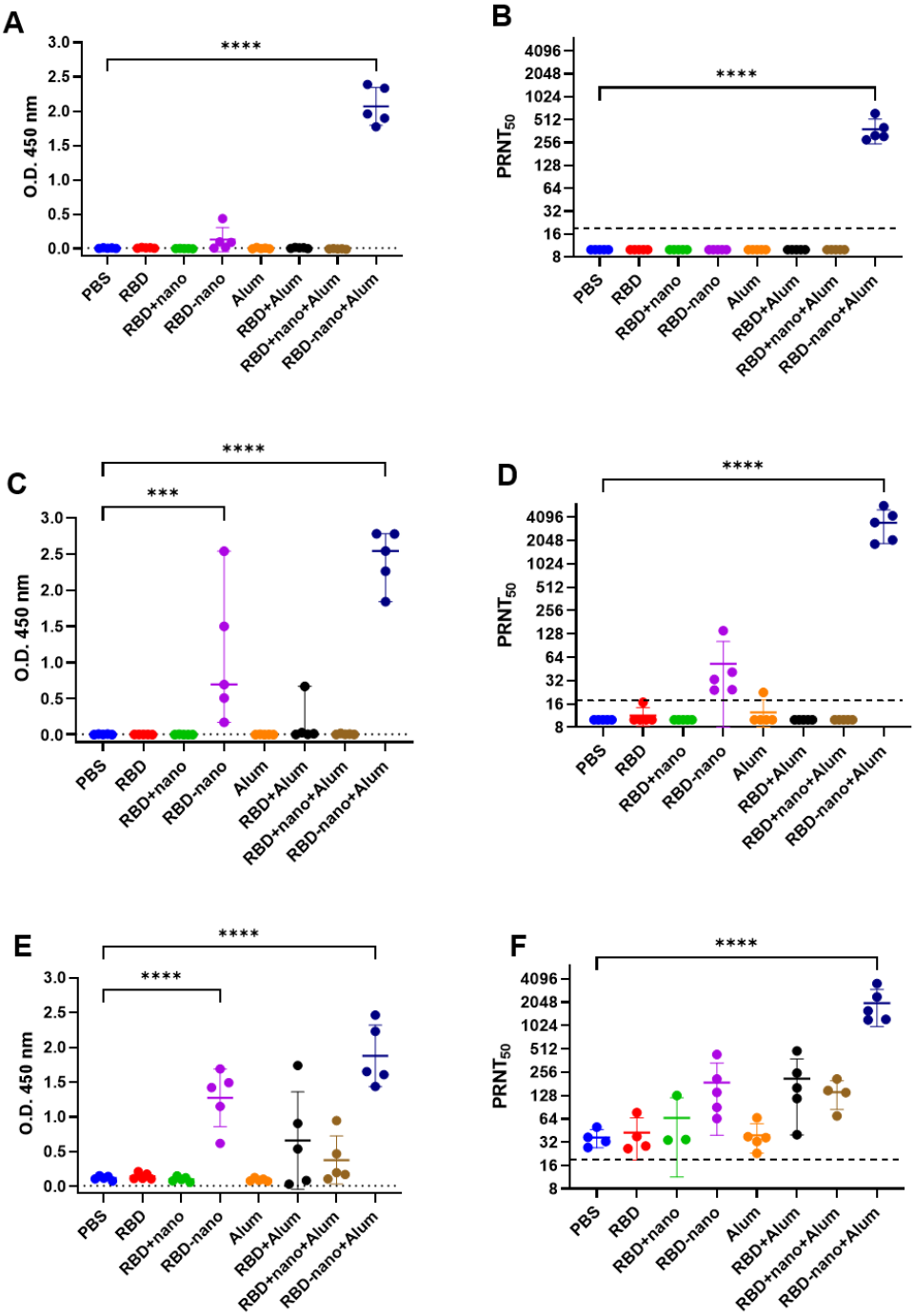

Figure 3

Figure 3

Figure 1.

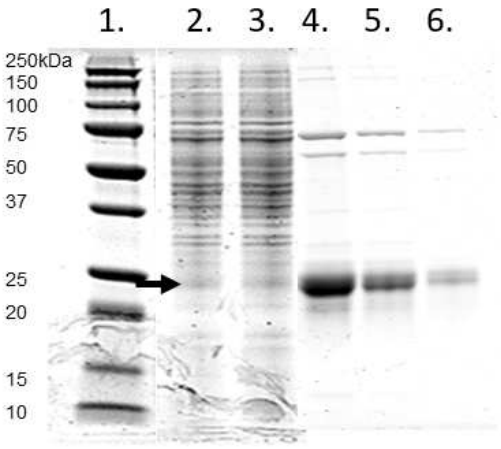

Figure 4

Figure 1

Figure 2.

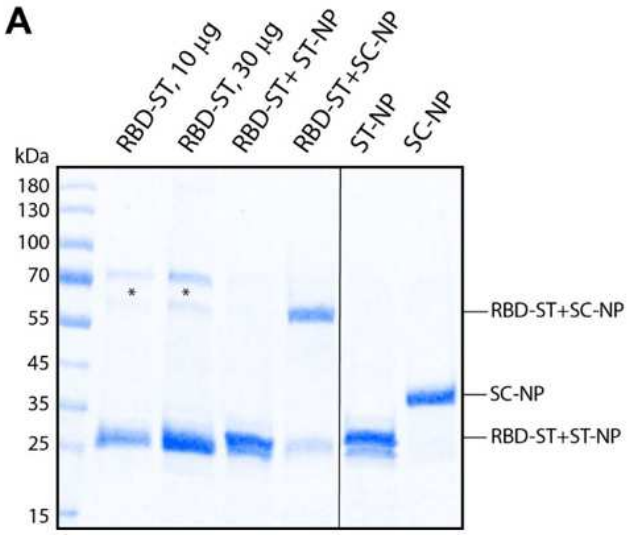

B

Group	Immunization
1	PBS
2	RBD
3	RBD + nanoparticle (RBD+nano)
4	RBD-nanoparticle coupled (RBD-nano)
5	Alum
6	RBD + Alum
7	RBD + nanoparticle + Alum (RBD+nano+Alum)
8	RBD-nanoparticle coupled + Alum (RBD-nano+Alum)

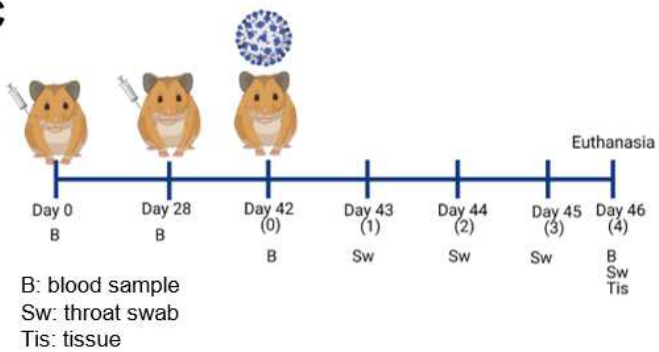

Figure 5

Figure 2

Figure 6.

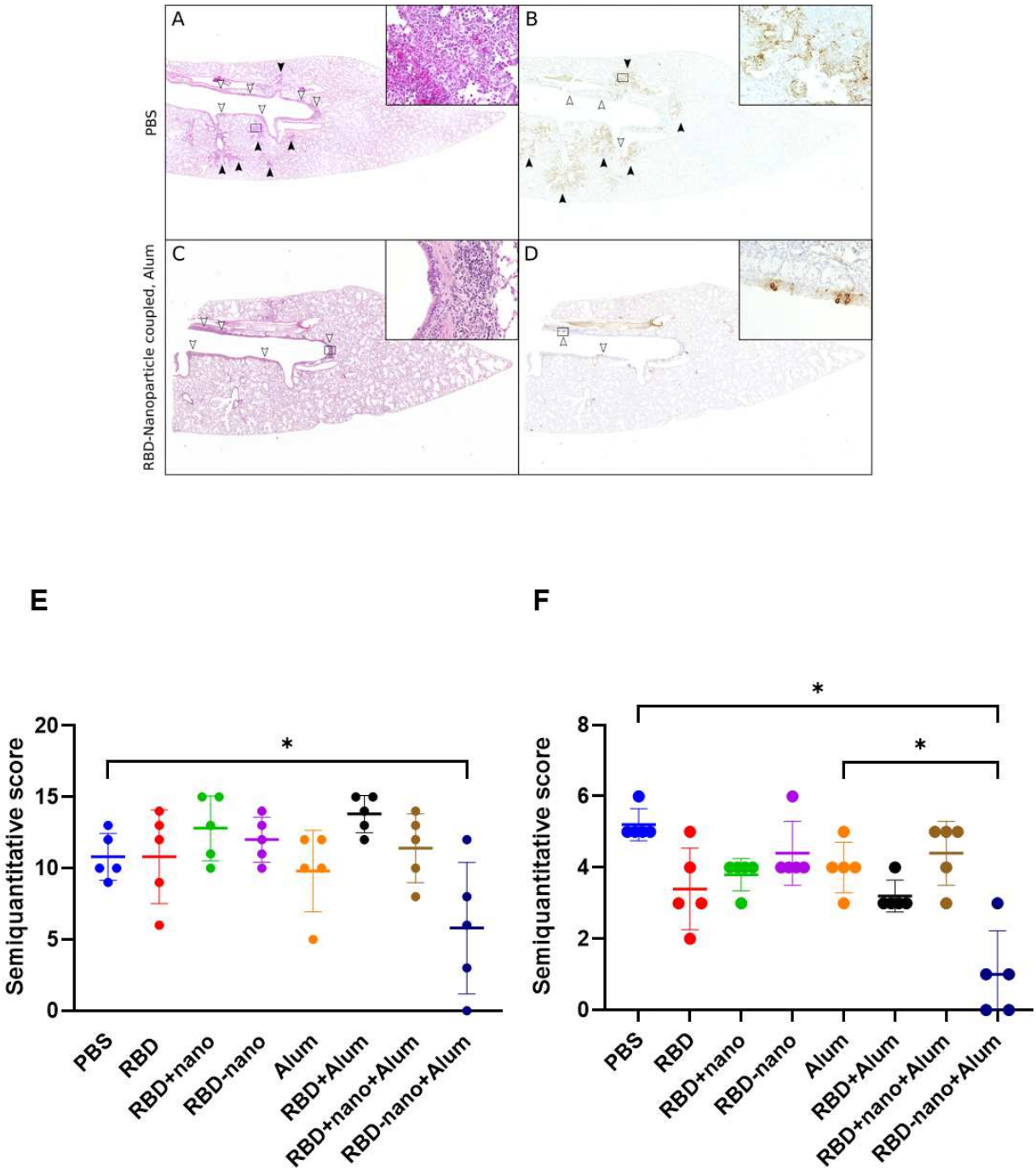

Figure 6

Figure 6